COMMUNICATION

A CaCO₃/nanocellulose-based bioinspired nacre-like material†

Masoud Farhadi-Khouzani,[a] Christina Schütz,[bc] Grażyna M. Durak,[a] Jordina Fornell,[d] Jordi Sort,[de] Germán Salazar-Alvarez,[bc] Lennart Bergström[bc] and Denis Gebauer*[a]

Nacre continues to be an inspiration for the fabrication of strong and tough materials from renewable and earth-abundant raw materials. Herein, we showed how a nacre-like hybrid material based on nanocellulose (NC) and CaCO₃ can be prepared *via* the sequential infiltration of polymer-stabilised CaCO₃ liquid precursors into layers of pre-deposited NC films. Layer-by-layer assembly of the NC films followed by controlled spreading and infiltration with liquid CaCO₃ precursors generated a lamellar material with an architecture and iridescent appearance similar to those of nacre. The wettability of the NC films towards the liquid CaCO₃ precursors was controlled by hydroxyl and carboxyl functionalization of the NC fibrils and the addition of magnesium ions. The combination of a high stiffness and plasticity of the nacre-like NC/CaCO₃ hybrid materials show that excellent mechanical properties can be obtained employing a fibrillar organic constituent that is relatively hard. The fabrication of a nacre-like hybrid material *via* an aqueous route of assembly and infiltration processing demonstrates how a sustainable composite material with outstanding properties can be produced using the most abundant biopolymer and biomineral on earth.

Introduction

In the quest for the development of materials with exceptional properties, biominerals fabricated by living organisms provide a vast source of inspiration. The properties of biominerals are diverse and relate to the combination of functions they serve in different organisms. The complex structures that have evolved to attain these specialized properties are genetically controlled and are formed under stringently controlled physiological conditions. Bone is a biomineral with exceptional mechanical properties conferred by the multilevel hierarchical structure of collagen and hydroxyapatite.[1] Another example of a material with intriguing mechanical properties is nacre. This iridescent and tough material protects the soft body of mollusks from predators and irritants and also serves as an outer layer of pearls.[2] Nacre is composed of 95% aragonite and 5% of mostly chitin,[3] where the remarkable fracture resistance stems from the 'brick and mortar' arrangement of the mineral and organic components.[4] In biological nacre, the hard mineral provides structural rigidity, whereas the soft organics dissipate fracture energy.[5] The biomineralization of calcium carbonate generally takes the advantage of amorphous calcium carbonate (ACC) as an intermediate to achieve the structurally complex combination of organic and inorganic constituents with a high degree of fidelity.[6,7] In bioinspired approaches, the great usefulness of droplets of liquid ACC stabilized by the presence of low amounts of polyanions, such as poly(aspartic acid), has been thoroughly demonstrated.[8,9] These so-called polymer-induced liquid precursors (PILPs; note that the polymer stabilizes the liquid precursors, rather than inducing them)[10–12] can be molded into any shape and thus enable the construction of tailor-made hybrids.[8,9,13,14] For instance, the successful *in vitro* re-mineralization of the biogenic insoluble matrix of nacre *via* PILPs suggests that this is also a viable pathway *in vivo*.[15] More recent work has demonstrated that polymer-mediated mineral growth in combination with a layer-by-layer deposition of porous organic films allowed the first replication of truly artificial nacre using CaCO₃.[16]

In this study, we combined the most abundant biomineral, calcium carbonate, with the most abundant biopolymer, cellulose, and demonstrated that a bioinspired synthesis route can be used to produce nacre-like laminated materials with outstanding mechanical properties. The structure consists of inexpensive materials, which are green and truly sustainable.

[a]Department of Chemistry, Physical Chemistry, University of Konstanz, Universitätsstr. 10, Box 714, D-78457 Konstanz, Germany. E-mail: denis.gebauer@uni-konstanz.de

[b]Department of Materials and Environmental Chemistry, Stockholm University, SE-10691 Stockholm, Sweden

[c]Wallenberg Wood Science Center, Teknikringen 56, SE-100 44 Stockholm, Sweden

[d]Departament de Física, Universitat Autonoma de Barcelona, E-08193 Bellaterra, Spain

[e]Institucio Catalana de Recerca i Estudis Avancats (ICREA), Pg. Lluís Companys 23, E-08010 Barcelona, Spain

16128 | *J. Mater. Chem. A*, 2017, 5, 16128–16133

This journal is © The Royal Society of Chemistry 2017

More specifically, we employed nanocellulose (NC)[17] that is a non-toxic, stiff, yet lightweight material with high tensile strength that is receiving rapidly increasing interest for the development of sustainable hybrid materials with excellent mechanical properties.[18–22] It has to be stressed that there are no previous examples of the successful combination of calcium carbonate and NC into a nacre-like structure as the bottom-up generation of an organic/inorganic-layered material with these compounds is highly challenging. This is due to the fact that none of the constituents provide an inherent 2D planar or scaffold basis, whereas a localized, controlled mineralization of the NC framework is required. Previous synthetic methods of other nacre-like materials involve predesigned matrix-directed mineralization,[23] electrophoretic deposition,[24,25] freeze casting,[26,27] templating,[15,27] layer-by-layer fabrication,[16,28,29] and self-assembly.[30–32] In this study, we showed that localized mineralization of deposited NC films by controlled spreading and imbibition of liquid $CaCO_3$ precursors allowed the processing of nacre-like materials with alternating layers of mineralized and unmineralized NC. Controlling the wettability[33] of NC with hydroxyl and carboxyl surface functionalization towards liquid $CaCO_3$ precursors in the presence and absence of magnesium, respectively, leads to a very high degree of compositional and structural fidelity of the NC/CaCO₃-based nacre-like material. Sequential assembly and infiltration is a facile and scalable method that can be used for the generation of multi-layered organic–inorganic nacre-like hybrids.

Results and discussion

Fig. 1(a) illustrates the protocol for the generation of the nacre-like material. A detailed description of the syntheses of the NC samples, the film preparations, and mineralization is provided in the ESI; Section S1-1–S1-5, including the choice of the suitable type of NC, control of film thickness, and PILP wettability on the given films. The morphology of the three different NC types used in this study is shown in the ESI, Fig. S1.† Films of NC functionalized with hydroxyl groups (NC–OH) and carboxyl groups (NC–COOH) are stable under the reaction conditions for $CaCO_3$ precipitation (high pH and initially 10 mM $CaCl_2$, ESI, Section S1-3 and Fig. S2†). Without Mg^{2+}, the NC–OH film shows very good wettability by $CaCO_3$ PILPs, whereas under the same conditions, NC–COOH cannot be wetted and thus remains unmineralized (ESI, Section S3-1-1 and Fig. S3–S5†). Under the chosen mineralization conditions, the ratio of the concentrations of calcium chloride and poly(aspartic acid) (ESI, Section S3-2 and Fig. S6–S8) are the key factors to obtain a homogenous coverage and infiltration of $CaCO_3$ for an initial NC film thickness below $ca.$ 1 μm.

Since the layer-by-layer technique requires a smooth base for further layering, obtaining a homogenous $CaCO_3$ mineralization is essential. In the kinetic setting of our mineralization procedure, the best mineralization results can be obtained from a NC dispersion with 0.11 wt% or less (ESI, Fig. S7–S9†), providing a suitable film thickness. With the established
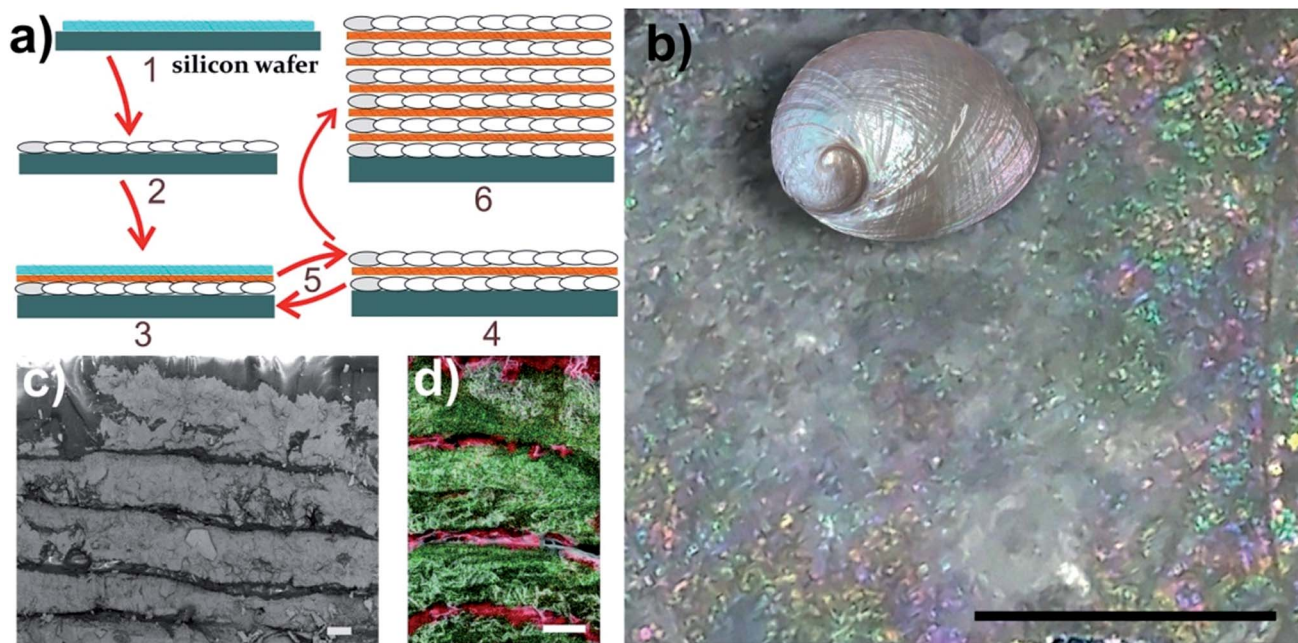
Fig. 1 (a) A schematic of the preparation protocol for the nacre-like material. (1) – Drop casting of the NC–OH layer on a silicon wafer. (2) – Mineralization of the NC–OH layer. (3) – Drop casting of one NC–COOH and one NC–OH layer on top of the mineralized NC–OH layer. (4) – Mineralization of the added NC–OH layer, but not the NC–COOH layer *via* controlled wettability. (5) – Repetition of steps (3) and (4) leads to a multi-layered material, which is composed of alternating mineralized and unmineralized NC layers – (6). (b) Image of a composite structure obtained after 18 mineralizations showing iridescence colors. The scale bar is 4 mm. The inset shows a polished abalone shell (*Haliotis laevigata*) with exposed iridescent nacre for comparison (not to scale). (c) SEM cross-section view of the layered structure. The scale bar is 10 μm (also see the ESI, Fig. S9†). (d) Overlay of the EDX mappings (Ca green and C red) of the cross-section of the nacre-like structure on the corresponding secondary electron image of the area, in which EDX was obtained (also see the ESI, Fig. S10†). The scale bar is 10 μm.

parameters, an initial mineralization of a single NC–OH layer was performed (Fig. 1(a)-2). SEM images of the surface of the mineralized sample with 750 nm thickness suggest that the individual crystals are mutually aligned (ESI, Fig. S9†), which is also apparent from the SAED pattern of the thin cuts (see below). Subsequently, a layer of NC–COOH followed by a layer of NC–OH was deposited, and then again mineralized (Fig. 1(a)-3). The latter mineralization procedure was repeated several times until an iridescent composite film was obtained (Fig. 1(b)). The iridescence can be interpreted as interference colors caused by the existence of multiple uniform layers.[34] Eighteen mineralizations provide a sufficient basis to create this pattern. Again, note that the key for the generation of the nacre mimic is the wetting and infiltration of the $CaCO_3$ PILPs on the NC–OH films and their mineralization, as opposed to the inter-layers of films of NC–COOH, which cannot be wetted in the absence of Mg^{2+} and remain unmineralized.

The obtained nacre-like material, based on the alternating organic and inorganic layers, was analyzed by scanning electron microscopy (SEM) techniques. The cross-section back-scattered electron (BSE) SEM image confirmed that the obtained material consists of layers of mineralized NC, which strongly backscatter the electrons and therefore appear much lighter than the unmineralized NC–COOH layers located between them (Fig. 1(c)

and ESI, Fig. S10†). The energy-dispersive X-ray spectroscopy (EDX) mapping of the cross-sections indicated that the distribution of Ca and C over the scanned area was concentrated within the NC–OH/$CaCO_3$ and NC–COOH layers, respectively (Fig. 1(d) and ESI Fig. S11†). Confocal laser scanning microscopy (CLSM) imaging of the NC component stained with Calcofluor White and combined with the collection of the light reflected from the mineral phase also confirmed the layered arrangement of the mineral/organic phases (ESI, Fig. S12†). To further analyze the mineralized parts, the samples were cut into sections with a microtome and analyzed by transmission electron microscopy (TEM) (Fig. 2(a and b), and ESI, Fig. S13†). The TEM image shows a layer of brick-like inter-connected crystals. Note that imaging under higher magnification resulted in the burning of the samples and hence it was not possible to improve the image quality any further. The selected area electron diffraction (SAED) pattern of the thin sections shows arcs, indicating that the crystals are mutually oriented (Fig. 2(c) and ESI, Fig. S13†). Evaluation of the SAED pattern reveals that these crystals are indeed calcite crystals, which are oriented in the [104] direction. Some of the reflections, which cannot be assigned to this calcite pattern with the zone axis [−441], are likely randomly oriented in other directions or may arise from NC.
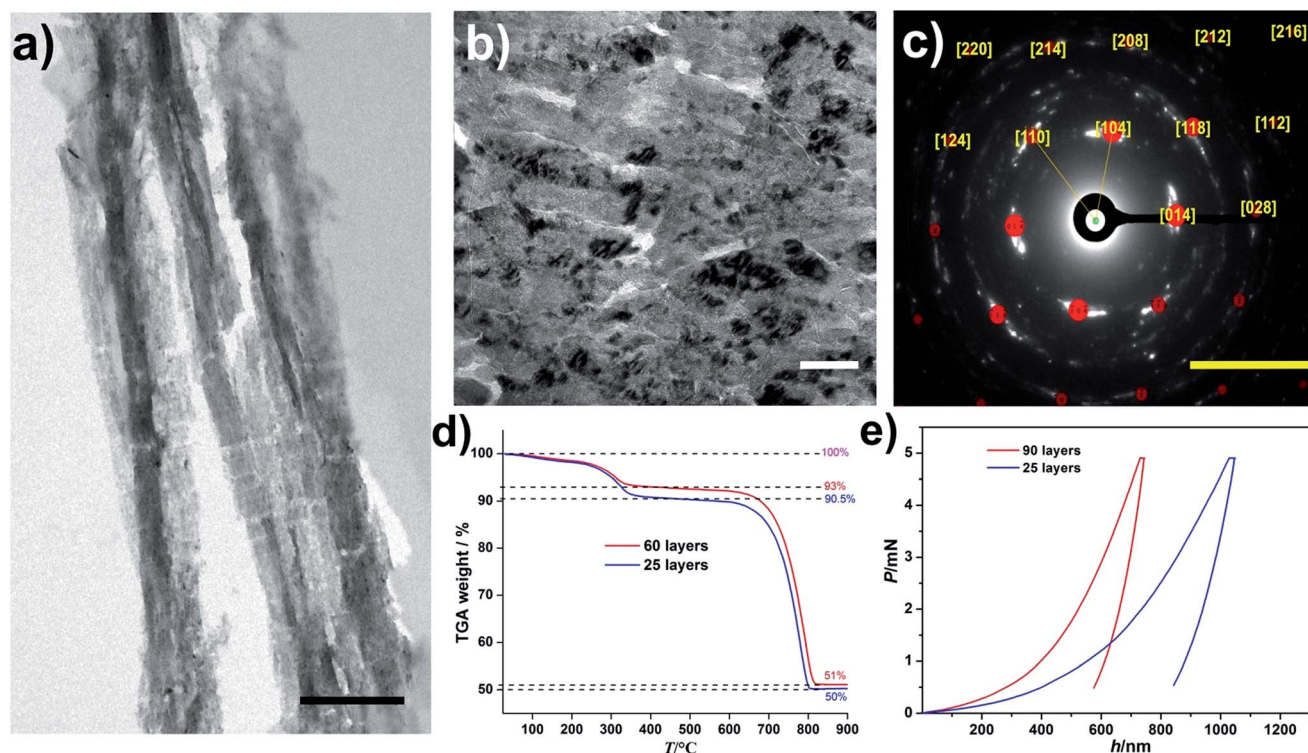

Fig. 2 (a and b) TEM images of a sample cross-section obtained by microtome cuts of the layered composite structure with mineralized NC−OH layers after 60 layers. Note that the ∼300 nm thin cuts were very sensitive towards the electron beam, leading to sample deterioration, especially of the NC constituents. Thus, the length scales of the mineralized and unmineralized layers established by SEM and confocal microscopy (Fig. 1c and d) are not directly evident. The scale bars are 1 μm and 100 nm in (a) and (b), respectively. (c) The SAED pattern of the area shown in (b). The yellow numbers assign the Miller indices to the different reflections corresponding to calcite crystals, which are oriented in the [104] direction, zone axis [−441]. The scale bar is 5 nm^{-1}. (d) TGA curves of the nacre mimics with different numbers of layers of the mineralized NC−OH as indicated. (e) Nanoindentation data showing the representative load (P) versus displacement (h) curves with a maximum applied force of 5 mN for different numbers of layers of the mineralized NC−OH as indicated.

16130 | J. Mater. Chem. A, 2017, 5, 16128–16133

This journal is © The Royal Society of Chemistry 2017

In any case, this mutual orientation of individual calcite crystals suggests that the mineralized inter-layers exhibit at least partly a mesocrystalline structure.[35] To determine the composition of the obtained materials, thermogravimetric analysis (TGA) was performed (Fig. 2(d)). The TGA of a sample with 60 layers shows two main plateaus where the first one occurs within the temperature range of 25–350 °C. A close assessment reveals a smooth mass loss (ca. 2%) below 250 °C, which was attributed to the loss of water. Note that the samples were incubated in a vacuum oven for 24 h before measuring the TGA curves. The existence of water in biogenic nacre was shown,[36] and herein, may be due to its trapping in the micropores resulting from the packing of the NC and is likely associated with the NC surface due to its highly hydrophilic character. Subtraction of the water content from the final mass loss towards this first plateau yields a fraction of organics of ca. 5%. The second major mass loss occurs between 650 and 830 °C and was attributed to the calcination of the $CaCO_3$ phase (ca. 93%). Interestingly, the resulting composition is very similar to that of the biological nacre.[37] The TGA of a sample with 25 layers gives value of 2%, 7.5%, and 92.5% for water, organics, and $CaCO_3$, respectively, and the minor differences between the 60- and 25-layers specimens illustrate that the bioinspired synthesis route yields a nacre-like material with a well-defined composition (Fig. 2(d)).

We also characterized the mechanical properties of the obtained nacre-like materials with different numbers of layers (Fig. 2(e) and ESI, Table S2†). The hardness of the composite increases with the increasing number of layers (Fig. 2(e)). The reduced Young's modulus of the composite with 90 layers was circa 14 GPa, which is similar to the value for human cortical bone[38] and exceeds the value of many nacre-like materials that are based on organic and inorganic constituents other than NC and $CaCO_3$ (reviewed and compiled in ref. 39). A quantitative comparison with the mechanical properties of different $CaCO_3$-based artificial nacre-like materials, also including biological examples of the nacreous layers of different abalone shells, is summarized in the ESI, Table S2.† Crack deflection by the plate-like crystals as well as crack trapping at the organic layers and the periodical variation of moduli are important for the impressive mechanical properties of biological nacre.[40] Because the NC/$CaCO_3$-layered hybrids are not built up by individual crystalline platelets, it is expected that the hardness and fracture toughness is lower than those of natural nacre. Mao et al. recently presented a $CaCO_3$-based nacre-like material with a platelet structure within the layers,[23] but note that also this material (ESI, Table S2†) was inferior to natural nacre. In the case of the present nacre-like hybrid, the fibrillar NC–OH within the mineralized layers can serve as a fiber-reinforcement,[41] where the tailored wetting of the liquid $CaCO_3$ precursors ensures the fiber-mineral adhesion. Nano-interconnectivity was highlighted to play a crucial role for the toughening and stiffening of nacre-like hybrids,[42] whereas any further synergistic toughening effects arising from the interfacial interactions of the building blocks, as in graphene oxide/NC-based nacre-like materials,[43,44] do not likely play a role.

The nacre-like material fabricated herein does indeed exhibit a large plasticity index (defined as the plastic indentation energy divided by the total indentation energy). This parameter provides an estimate of how much energy can be absorbed by the material during, for example, an impact. It is relatively high for the NC/$CaCO_3$ nacre-like hybrid, and noteworthy, even higher than for the biological nacreous layer of Haliotis laevigata (ESI, Table S2†).

It is also interesting to compare the material properties of the nacre-like material to another example of transparent hybrid films composed of NC and nanoparticles of amorphous $CaCO_3$ (ACC).[18] While the hardness of the nacre-like hybrid and the transparent hybrid materials are similar, the reduced Young's modulus of the nacre-like structure was larger. This is likely due to the morphology of the hybrids, where the more organized and ordered structure of the nacre-like material was stiffer. However, calcite with a mesocrystalline structure comprises the nacre-like structure (see above), as opposed to the transparent hybrid film that contained only ACC, which may also play a role in this context.

When the mineralizations were carried out under appropriate conditions in the presence of Mg^{2+}, the wettability of the distinct films with $CaCO_3$ PILPs is inverted, i.e., the NC–COOH film can be mineralized as opposed to the NC–OH films (ESI, Fig. S14 and S15†). Moreover, the inorganic constituent is then not calcite, but ACC (ESI, Fig. S14;† see Section S3-3 for further discussions).[45]

Conclusions

In conclusion, by controlling the reaction conditions and in particular, the wettability of NC–OH and NC–COOH towards PILPs in the absence and in the presence of magnesium ions, respectively, a layered hybrid material containing ca. 90% calcite exhibiting mesocrystalline features can be generated. The resulting nacre-like, iridescent structure shows mineralized parts with a thickness of ca. 20 μm separated by layers of unmineralized NC–COOH with a thickness of ca. 1 μm. The composition of the $CaCO_3$-NC laminates is very similar to that of nacre, which suggests that the PILP-based mineralization pathway on organic matrices with a tunable wettability has a strong resemblance to the mineralization process occurring in living organisms.[46] The mechanical properties of the obtained structure reveal a relatively hard material with a reduced Young's modulus, similar to cortical bone, and a high plasticity—surpassing biological nacre—that is likely based upon NC-fiber-reinforced, mesocrystalline $CaCO_3$. The bio-inspired mineralization strategy is of interest to a wide range of materials also beyond NC with potential applications in e.g., packaging and building industries. The level of control over the localization of mineralization sites can be employed for the generation of even more complex patterns in hybrid materials, e.g., based on the phase behavior of NC[47] or self-assembled organic frameworks.

Acknowledgements

References

1 U. Tritschler and H. Cölfen, *Bioinspiration Biomimetics*, 2016, **11**, 035002.

2 J. Y. Sun and B. Bhushan, *RSC Adv.*, 2012, **2**, 7617–7632.

3 H. D. Espinosa, J. E. Rim, F. Barthelat and M. J. Buehler, *Prog. Mater. Sci.*, 2009, **54**, 1059–1100.

4 H. A. Lowenstam and S. Weiner, *On biomineralization*, Oxford University Press, New York, 1989.

5 H. J. Gao, *Int. J. Fract.*, 2006, **138**, 101–137.

6 L. Addadi, D. Joester, F. Nudelman and S. Weiner, *Chem.–Eur. J.*, 2006, **12**, 981–987.

7 H. B. Yao, J. Ge, L. B. Mao, Y. X. Yan and S. H. Yu, *Adv. Mater.*, 2014, **26**, 163–188.

8 L. B. Gower, *Chem. Rev.*, 2008, **108**, 4551–4627.

9 D. Gebauer, M. Kellermeier, J. D. Gale, L. Bergström and H. Cölfen, *Chem. Soc. Rev.*, 2014, **43**, 2348–2371.

10 S. E. Wolf, J. Leiterer, M. Kappl, F. Emmerling and W. Tremel, *J. Am. Chem. Soc.*, 2008, **130**, 12342–12347.

11 M. A. Bewernitz, D. Gebauer, J. Long, H. Cölfen and L. B. Gower, *Faraday Discuss.*, 2012, **159**, 291–312.

12 F. Sebastiani, S. L. Wolf, B. Born, T. Q. Luong, H. Cölfen, D. Gebauer and M. Havenith, *Angew. Chem., Int. Ed.*, 2017, **56**, 490–495.

13 S. J. Homeijer, R. A. Barrett and L. B. Gower, *Cryst. Growth Des.*, 2010, **10**, 1040–1052.

14 S. S. Jee, T. T. Thula and L. B. Gower, *Acta Biomater.*, 2010, **6**, 3676–3686.

15 N. Gehrke, N. Nassif, N. Pinna, M. Antonietti, H. S. Gupta and H. Cölfen, *Chem. Mater.*, 2005, **17**, 6514–6516.

16 A. Finnemore, P. Cunha, T. Shean, S. Vignolini, S. Guldin, M. Oyen and U. Steiner, *Nat. Commun.*, 2012, **3**, 966.

17 C. Salas, T. Nypelo, C. Rodriguez-Abreu, C. Carrillo and O. J. Rojas, *Curr. Opin. Colloid Interface Sci.*, 2014, **19**, 383–396.

18 D. Gebauer, V. Oliynyk, M. Salajkova, J. Sort, Q. Zhou, L. Bergström and G. Salazar-Alvarez, *Nanoscale*, 2011, **3**, 3563–3566.

19 B. Wicklein, A. Kocjan, G. Salazar-Alvarez, F. Carosio, G. Camino, M. Antonietti and L. Bergström, *Nat. Nanotechnol.*, 2015, **10**, 277–283.

20 X. Yang, K. Y. Shi, I. Zhitomirsky and E. D. Cranston, *Adv. Mater.*, 2015, **27**, 6104–6109.

21 M. Ishikawa, Y. Oaki, Y. Tanaka, H. Kakisawa, G. Salazar-Alvarez and H. Imai, *J. Mater. Chem. B*, 2015, **3**, 5858–5863.

22 C. Schütz, J. Sort, Z. Bacsik, V. Oliynyk, E. Pellicer, A. Fall, L. Wågberg, L. Berglund, L. Bergström and G. Salazar-Alvarez, *PLoS One*, 2012, **7**, 10.

23 L. B. Mao, H. L. Gao, H. B. Yao, L. Liu, H. Cölfen, G. Liu, S. M. Chen, S. K. Li, Y. X. Yan, Y. Y. Liu and S. H. Yu, *Science*, 2016, **354**, 107–110.

24 C. A. Wang, B. Long, W. Lin, Y. Huang and J. Sun, *J. Mater. Res.*, 2008, **23**, 1706–1712.

25 W. Lin, C. A. Wang, H. L. Le, B. Long and Y. Huang, *Mater. Sci. Eng., C*, 2008, **28**, 1031–1037.

26 E. Munch, M. E. Launey, D. H. Alsem, E. Saiz, A. P. Tomsia and R. O. Ritchie, *Science*, 2008, **322**, 1516–1520.

27 H. Bai, F. Walsh, B. Gludovatz, B. Delattre, C. L. Huang, Y. Chen, A. P. Tomsia and R. O. Ritchie, *Adv. Mater.*, 2016, **28**, 50–56.

28 P. Podsiadlo, M. Michel, K. Critchley, S. Srivastava, M. Qin, J. W. Lee, E. Verploegen, A. J. Hart, Y. Qi and N. A. Kotov, *Angew. Chem., Int. Ed.*, 2009, **48**, 7073–7077.

29 H. Wei, N. Ma, F. Shi, Z. Q. Wang and X. Zhang, *Chem. Mater.*, 2007, **19**, 1974–1978.

30 P. Das, J. M. Malho, K. Rahimi, F. H. Schacher, B. C. Wang, D. E. Demco and A. Walther, *Nat. Commun.*, 2015, **6**, 5967.

31 B. L. Zhu, N. Jasinski, A. Benitez, M. Noack, D. Park, A. S. Goldmann, C. Barner-Kowollik and A. Walther, *Angew. Chem., Int. Ed.*, 2015, **54**, 8653–8657.

32 A. Walther, I. Bjurhager, J. M. Malho, J. Pere, J. Ruokolainen, L. A. Berglund and O. Ikkala, *Nano Lett.*, 2010, **10**, 2742–2748.

33 J. K. Berg, T. Jordan, Y. Binder, H. G. Börner and D. Gebauer, *J. Am. Chem. Soc.*, 2013, **135**, 12512–12515.

34 T. L. Tan, D. Wong and P. Lee, *Opt. Express*, 2004, **12**, 4847–4854.

35 L. Bergström, E. V. Sturm, G. Salazar-Alvarez and H. Cölfen, *Acc. Chem. Res.*, 2015, **48**, 1391–1402.

36 D. Verma, K. Katti and D. Katti, *Spectrochim. Acta, Part A*, 2007, **67**, 784–788.

37 X. Bourrat, L. Francke, E. Lopez, M. Rousseau, P. Stempflé, M. Angellier and P. Albéric, *CrystEngComm*, 2007, **9**, 1205–1208.

38 J. Y. Rho, R. B. Ashman and C. H. Turner, *J. Biomech.*, 1993, **26**, 111–119.

39 J. F. Wang, Q. F. Cheng and Z. Y. Tang, *Chem. Soc. Rev.*, 2012, **41**, 1111–1129.

40 Y. Shao, H. P. Zhao, X. Q. Feng and H. J. Gao, *J. Mech. Phys. Solids*, 2012, **60**, 1400–1419.

41 A. K. Bledzki and J. Gassan, *Prog. Polym. Sci.*, 1999, **24**, 221–274.

42 M. Grossman, F. Bouville, F. Erni, K. Masania, R. Libanori and A. R. Studart, *Adv. Mater.*, 2016, 1605039, DOI: 10.1002/adma.201605039.

43 S. Gong, L. Jiang and Q. F. Cheng, *J. Mater. Chem. A*, 2016, **4**, 17073–17079.

16132 | *J. Mater. Chem. A*, 2017, **5**, 16128–16133

This journal is © The Royal Society of Chemistry 2017

44 W. Cui, M. Z. Li, J. Y. Liu, B. Wang, C. Zhang, L. Jiang and Q. F. Cheng, *ACS Nano*, 2014, **8**, 9511–9517.

45 Y. Politi, D. R. Batchelor, P. Zaslansky, B. F. Chmelka, J. C. Weaver, I. Sagi, S. Weiner and L. Addadi, *Chem. Mater.*, 2010, **22**, 161–166.

46 S. E. Wolf, I. Lieberwirth, F. Natalio, J. F. Bardeau, N. Delorme, F. Emmerling, R. Barrea, M. Kappl and F. Marin, *Faraday Discuss.*, 2012, **159**, 433–448.

47 J. P. F. Lagerwall, C. Schütz, M. Salajkova, J. Noh, J. H. Park, G. Scalia and L. Bergström, *NPG Asia Mater.*, 2014, **6**, e80.

This journal is © The Royal Society of Chemistry 2017

J. Mater. Chem. A, 2017, **5**, 16128–16133 | **16133**